FORCED FLAPPING BEHAVIOUR OF AN ORNICOPTER ROTOR BLADE

Dennis van Gerwen[1], Monique Heiligers[2], Theo van Holten[3]

[1] Delft University of Technology
Kluyverweg 1, 2629 HS Delft, The Netherlands
e-mail: d.j.vangerwen@tudelft.nl

[2] Delft University of Technology
Kluyverweg 1, 2629 HS Delft, The Netherlands
e-mail: m.m.heiligers@tudelft.nl

[3] Delft University of Technology
Kluyverweg 1, 2629 HS Delft, The Netherlands
e-mail: th.vanholten@tudelft.nl

Key words: Ornicopter, flapping, rotor blade, finite element

Abstract. The Ornicopter is a single rotor helicopter without a reaction torque. The single rotor provides full flight control capabilities, hence a tail rotor is not required. This is achieved by forcing the rotor blades to flap up and down once per revolution. By flapping the blades up and down in a controlled manner, the aerodynamic forces that act on the rotor blade are used to drive the rotation of the rotor. Thus no torque needs to be applied to the rotor shaft, and as a result, no reaction torque will arise.
The forced flapping motion of the rotor blades is generated by a so called flapping mechanism. The dimensions of such a mechanism depend directly on the amplitude of the forced flapping motion required for torqueless rotation of the rotor. Hence an accurate prediction of the amplitude of the forced flapping motion required is very important. Furthermore, the effect of forced flapping on the stress distribution in a rotor blade needs to be investigated in order to design rotor blades suitable for the Ornicopter.
Rigid blade theory is available for the prediction of flapping amplitudes and in addition a modal superposition approach has also been developed. However, experiments have shown that these theories do not predict the flapping amplitude with sufficient accuracy. Furthermore, these methods do not yield satisfactory information about stress distributions in the rotor blade.
This paper presents an alternative method for analyzing the forced flapping motion of an Ornicopter rotor blade. The method employs an existing planar beam finite element for geometrically nonlinear dynamic analysis. Simple external force models are presented for the centrifugal load and for the aerodynamic loads. The method is validated by comparing the results with experimental data obtained from a radio controlled Ornicopter demonstrator model. Finally the method is used to analyze two different flapping load cases for a full size rotor blade based on a Schweizer 300C helicopter blade.

NOTATIONS

A	Cross-sectional area
A_s	Shear reduced area
c	Blade chord
$\overline{C}_{d_p}$	Average profile drag coefficient
$\overline{C}_{l_\alpha}$	Average lift slope
$\underline{D}_e$	Global element displacement vector
$\underline{d}_e$	Local element displacement vector
D_m	Drag evaluated at element center
E	Modulus of elasticity
EI_z	Flexural rigidity
$\underline{F}_e$	Element external force vector
$\underline{F}_{e,aero}$	Element aerodynamic force vector
$\underline{F}_{e,centr}$	Element centrifugal force vector
F_{fl}	Flapping force
G	Shear modulus
I	Mass moment of inertia
I_z	Area moment of inertia of cross-section
k	Induced power correction factor
$\mathbf{k}_0$	Element stiffness matrix (local)
$\underline{K}_e$	Element internal force vector
l_0	Undeformed element length
L_m	Lift evaluated at element center
m	Mass per unit length
$\mathbf{M}_e$	Element mass matrix (global)
$\hat{m}_{fl}$	Amplitude of nondimensional flapping moment
M_{fl}	Flapping moment
N	Number of rotor blades
N_m	Aerodynamic component normal to element, evaluated at element center
P_{fl}	Flapping power
P_i	Induced power
P_p	Profile drag power
P_{sh}	Rotor shaft power
$\overline{Q}_{sh}$	Average rotor shaft torque
$Q_{sh,e}$	Shaft torque due to element
R	Rotor radius
T	Rotor thrust
T_m	Aerodynamic component parallel to shaft plane, evaluated at element center
u	Displacement in local x-direction
U	Displacement in global X-direction
v	Displacement in local y-direction
V	Displacement in global Y-direction
V_m	Airspeed evaluated at element center
X	Global X-coordinate
X_m	Global X-coordinate of element center
α	Angle of attack
β	Rigid blade flapping angle
$\hat{\beta}$	Rigid blade flapping angle amplitude
β_{RBF}	Residual bending flexibility correction
γ	Lock number
$\hat{\varepsilon}$	Flexible blade root angle amplitude
ρ	Air density
σ	Rotor solidity
θ	Global element orientation
θ_0	Collective pitch angle
φ	Local inflow angle
ϕ	Local cross section orientation
Φ	Global cross section orientation
Ω	Rotor rotational speed

1 INTRODUCTION: A SINGLE ROTOR HELICOPTER WITHOUT REACTION TORQUE

The helicopter tail rotor has always been considered a necessary evil. Without it, a conventional helicopter would be uncontrollable. Yet the tail rotor is an expensive contraption, it consumes a lot of power yielding nothing in return and it provides only marginal control authority under unfavourable wind conditions. On top of that, it is noisy, vulnerable and dangerous. The ideal solution to all these problems would be to design a main rotor that eliminates the need for a tail rotor.
The Ornicopter is such a revolutionary design. The Ornicopter is a helicopter that is fully controlled using only a single (main) rotor.

1.1 Forced flapping of the rotor blades

The Ornicopter principle is based on bird flight. Birds are able to generate both a lifting force and a propelling force by flapping their wings. The movement of a bird wing however is extremely complicated and it is impossible to accurately mimick this movement using an Ornicopter blade. Nevertheless a very useful and simple approximation can be obtained by forcing the Ornicopter blade to flap up and down at a constant pitch angle.

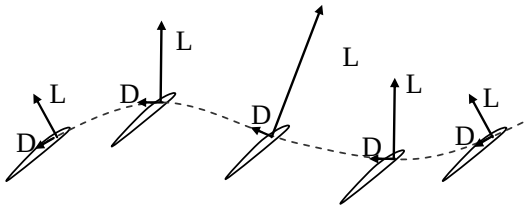

Figure 1: Lift and drag forces acting on an Ornicopter blade element during one revolution when a constant collective pitch angle is applied

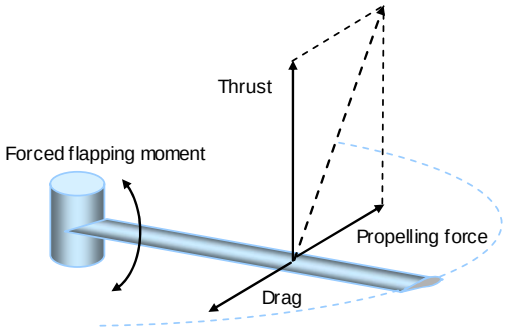

Figure 2: Due to forced flapping, part of the aerodynamic resultant is used to propel the Onricopter rotor blade

The movement of an Ornicopter blade during one revolution is depicted in Figure 1. During one revolution of the blade, the blade is forced to flap both up and down once, resulting in the undulating path shown. If a constant pitch angle is applied the aerodynamic forces will (averaged over one revolution) result in an upward force and a propulsive force that counteracts the blade drag. This propulsive force is achieved because the forward horizontal component of the lift force that occurs when the blade is flapping downwards is much larger than the backward horizontal component of the lift force that occurs when the blade is flapping upwards. Thus by setting all the Ornicopter blades at a constant pitch angle and flapping them up and down, a propulsive force is created that will rotate the blades around the rotor hub and an upward force is created that will counteract gravity (Figure 2).

1.2 Absence of a reaction torque

So why is it that, when the blades are propelled by a flapping motion, there is no reaction torque acting on the fuselage? This can be explained by comparing a conventional helicopter with an Ornicopter.

In a conventional helicopter, rotor blade drag is counteracted by the torque that is exerted on the rotor shaft, as depicted in Figure 3. The rotor thus rotates due to the torque that is transferred from the fuselage to the rotor. As a result there will also be a reaction torque from the rotor on the fuselage, and this reaction torque will have to be counteracted by an anti-torque device.
For the Ornicopter configuration the drag acting on the rotor blades is counteracted by the propelling force produced by the forced flapping motion of the blade, as depicted in Figure 4. Thus no direct torque is transferred from the fuselage to the rotor. As a consequence there will neither be a reaction torque from the rotor on the fuselage. And hence an anti-torque device (tail rotor) is no longer necessary.

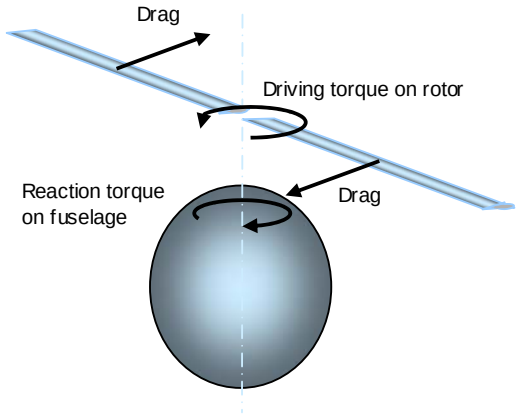

Figure 3: Forces and moments acting on a conventional helicopter

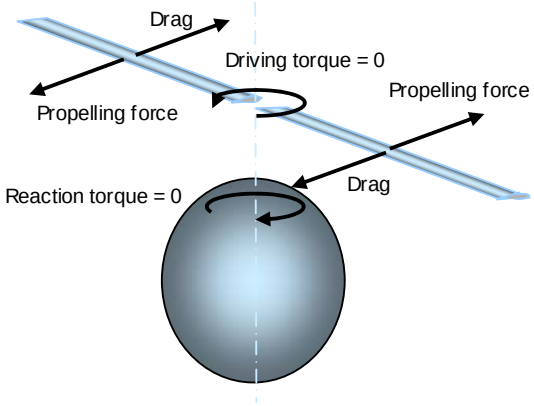

Figure 4: Forces and moments acting on an Ornicopter

1.3 Flapping mechanism and yaw control

Obviously some mechanism is required in order to generate the forced flapping motion of the rotor blades, that is, to convert engine power into flapping power. This is referred to as the flapping mechanism. An example of such a flapping mechanism, as implemented in the experimental radio controlled Ornicopter demonstrator model, is depicted in Figure 8.
The most straightforward way to provide flapping power to the rotor blades is via the rotor shaft. By directly coupling the flapping mechanism to the rotor shaft, a 1-P (once per revolution) flapping motion is achieved, taking advantage of resonance. There is somewhat of a paradox here, because a torque is applied to the rotor shaft in order to prevent a reaction torque from arising. This can be explained as follows.
As with a conventional helicopter, the engine applies a torque to the rotor shaft, which in turn causes the rotor to rotate. However, due to the presence of a flapping mechanism, part of the power applied to the shaft is used to flap the blades up and down. The amount of power diverted to this flapping motion is directly related to the amplitude of the flapping motion, which can be controlled with the help of the flapping mechanism. Now, if the correct flapping amplitude is chosen for a constant power setting, the amount of power used for flapping will be equal to the amount of power transferred to the rotor shaft by the engine, and as a result the torque applied to the shaft will be fully counteracted within the flapping mechanism. The net result is that the rotor is now driven by the forced flapping of the blades only.
This way of transferring flapping power to the rotor blades has another advantage. At constant power setting, a small deviation from the equilibrium flapping amplitude implies that power required for flapping becomes larger or smaller than the power transferred to the rotor shaft.

As a result a small reaction torque will arise. Thus by manipulating the flapping amplitude, the amount of reaction torque and the direction of the reaction torque can be controlled. Hence the forced flapping amplitude is a control variable, taking over the role of tail rotor pitch in conventional helicopters.

1.4 Basic Ornicopter theory

During the past couple of years, research has mainly been focused on developing and studying the underlying theory of the Ornicopter [1][2][3][4][5]. A thorough understanding of this theory is necessary in order to be able to understand the effects of forced flapping on rotor performance, rotor loads, vibrations etc. The basic theoretical model for the Ornicopter is based on rigid blade theory. A short summary of the theory described by [2] is given here.

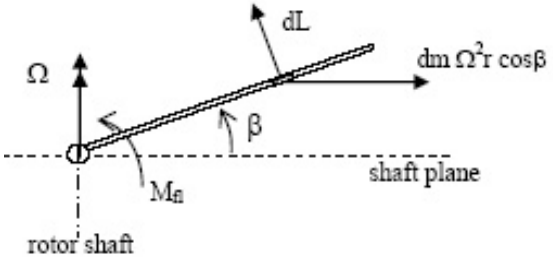

Figure 5: Centrally hinged rigid blade model with root flapping moment

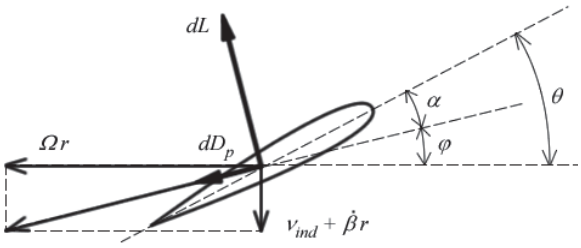

Figure 6: Flow components and aerodynamic forces acting on a blade element at distance r from the shaft

The forced flapping principle is best illustrated using a centrally hinged, uniform, rigid blade at constant rotor rotational speed in hover condition. Based on the model depicted in Figure 5 and Figure 6 with a flapping moment M_{fl} applied at the root, the following expression for the rotor shaft power can be derived:

$$P_{sh} = P_i + P_p - P_{fl} \tag{1}$$

where $P_{fl} = NP_{fl,b}$ is the total flapping power for N blades, P_i is the induced drag power;

$$P_i = kT\sqrt{\frac{T}{2\rho\pi R^2}} \tag{2}$$

and P_p is the profile drag power;

$$P_p = \tfrac{1}{8}\overline{C}_{D_p}\rho\sigma(\Omega R)^3\pi R^2 \tag{3}$$

In these expressions, k is the induced power correction factor, T is the rotor thrust in hover, ρ is the air density, R is the rotor radius, $\overline{C}_{D_p}$ is the average profile drag coefficient and $\sigma = Nc/(\pi R)$ is the rotor solidity.

The power that goes into forced flapping for a single blade is found with the help of blade element theory [2] to be equal to:

$$P_{fl,b} = \frac{I\Omega^3\gamma}{16}\hat{\beta}^2 \tag{4}$$

where I is the mass moment of inertia of the blade with respect to the flapping hinge, Ω is the rotor speed, $\gamma = \rho\overline{C}_{l,\alpha}cR^4/I$ is the Lock number, where $\overline{C}_{l,\alpha}$ is the average lift slope and c is the blade chord, and $\hat{\beta}$ is the forced flapping amplitude.

The average shaft torque at constant rotor speed can then be expressed as:

$$\overline{Q}_{sh} = \frac{P_{sh}}{\Omega} = \frac{P_i + P_p - NP_{fl,b}}{\Omega} \tag{5}$$

Hence in order to reduce the average shaft torque to zero, the flapping power should equal the sum of induced drag power and profile drag power.

The flapping amplitude $\hat{\beta}$ required for torqueless rotation ($\overline{Q}_{sh} = 0$) is therefore:

$$\hat{\beta} = \sqrt{\frac{16(P_i + P_p)}{NI\Omega^3\gamma}} \tag{6}$$

The corresponding non-dimensional flapping moment is:

$$\hat{m}_{fl} = \frac{\gamma}{8}\hat{\beta} \tag{7}$$

These expressions for the rigid blade flapping amplitude and corresponding flapping moment could be used as a first approximation in the preliminary design process of a flapping mechanism.

However, because the size of a flapping mechanism is directly determined by the flapping amplitude, accuracy of the prediction is very important. Experiments with an Ornicopter wind tunnel model and with the radio controlled Ornicopter demonstrator model [6], which is depicted in Figure 7 and Figure 8, have shown that the actual flapping amplitude (measured at the flapping hinge) required for torqueless rotation is much larger than the one predicted using Equation 6. This could be expected because an actual rotor blade is flexible and will therefore deform under the influence of the flapping loads. The qualitative effect of blade flexibility on root flapping angle is illustrated by Figure 9.

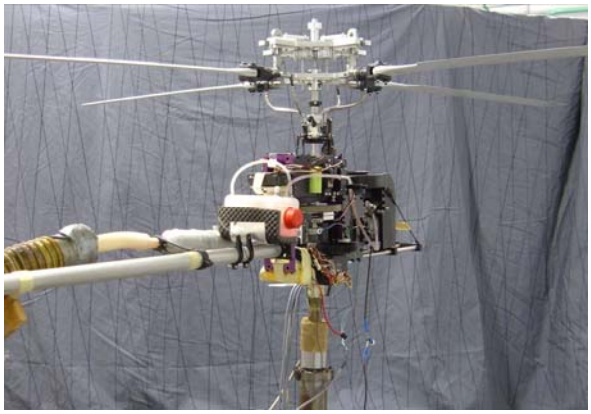

Figure 7: The radio controlled Ornicopter demonstrator model on a fixed base test stand equipped with strain gauges [6]

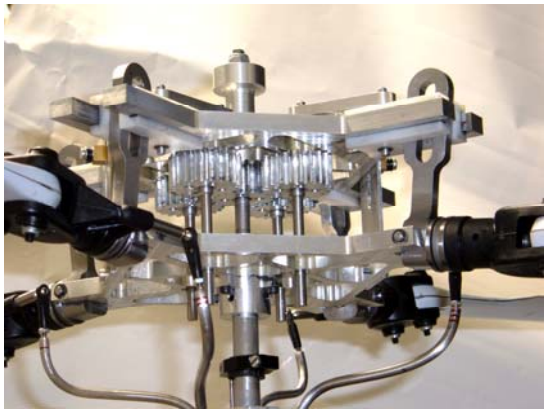

Figure 8: Close-up of the flapping mechanism of the radio controlled Ornicopter demonstrator model

1.5 Rigid blade theory vs. Flexible blade theory

The influence of blade flexibility has been investigated by [4] using a modal superposition method. A two-mode approximation (rigid body mode and first bending mode) of a centrally hinged blade in zero-lift condition with a flapping moment applied at the root yields considerably better results than rigid blade theory, as far as the root flapping amplitude is concerned.

According to [4] the root flapping amplitude required for a flexible blade ($\hat{\varepsilon}$) is much larger than that for a rigid blade ($\hat{\beta}$), but on the other hand the root flapping moment for the flexible

blade is smaller. However, the amount of power required for flapping is not influenced by blade flexibility (when neglecting structural damping).
To illustrate the effect of blade flexibility on flapping requirements, the rigid blade prediction of the flapping amplitude required for the Ornicopter demonstrator model in the zero-lift condition is depicted in Figure 10, together with the flexible blade prediction, as a function of rotor speed.

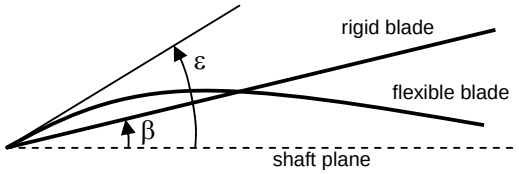

Figure 9: Root flapping angle for a rigid blade (β) and for a flexible blade (ε)

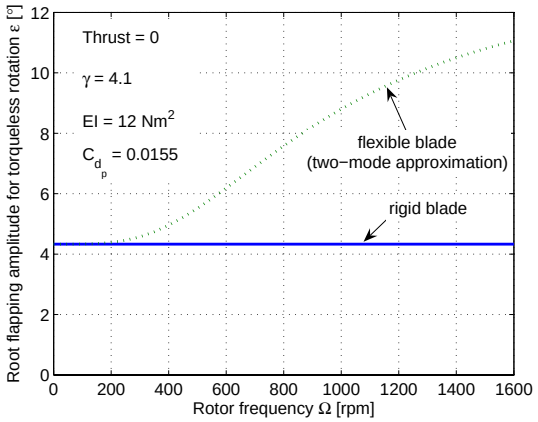

Figure 10: The effect of blade flexibility on the root flapping amplitude required for torqueless rotation for the Ornicopter demonstrator model at zero lift

The size of an Ornicopter flapping mechanism is proportional to the flapping amplitude. This makes the flapping amplitude a major design driver for the Ornicopter. Hence an accurate prediction of the actual root flapping angle required for torqueless rotation is very important, even in the preliminary design phase.
Furthermore, the stress distribution in the rotor blade due to forced flapping loads needs to be determined if a suitable rotor blade is to be designed for use on an Ornicopter.
Rigid blade theory, although very useful for basic performance calculations, is not applicable here. The modal summation method on the other hand does yield reasonable accuracy for the zero lift condition, but application to lifting conditions and other load cases requires a lot of effort and the results are yet to be proven.
All in all, there is reason enough to look into another method of rotor blade analysis.

2 A FINITE ELEMENT APPROACH TO FORCED FLAPPING

As an alternative to the analytical methods, a geometrically nonlinear finite element (FE) method has been employed in order to allow a more detailed analysis of rotor blade behaviour under forced flapping conditions. This has several advantages over the analytical methods, for example: analysis of non-uniform structures is relatively easy, flapping mechanism geometry can be taken into account and the stress distribution in the blade can be investigated.
The finite element method employed is based on the planar beam element developed by [8]. The resulting FE rotor blade model is discussed next.

2.1 A planar Timoshenko beam element for large rotations

The planar beam element presented by [8] is a standard Timoshenko beam for small deflections, applied in a type of co-rotational formulation. This implies that the element is

subject to rigid body rotation and deformations are calculated with respect to the rotated configuration. This way, assuming that the elements are small enough, deformations (strains) can remain small, which justifies the use of linear elastic theory.
The Timoshenko beam element is different from the well known Euler-Bernoulli element (also known as EBT, engineering bending theory) in that it takes into account the effects of shear deformation on bending behaviour, as depicted in Figure 11. The orientation of a cross-section of the Timoshenko element is independent of the deflection, allowing the use of linear shape functions for the deformations U, V and Φ (Figure 13), which simplifies calculations considerably (whereas in EBT, the cross-sections remain perpendicular to the neutral line, making ϕ dependent on v and thus requiring a higher order shape function for ϕ). The deformed Timoshenko element thus remains straight, as can be seen in Figure 11.

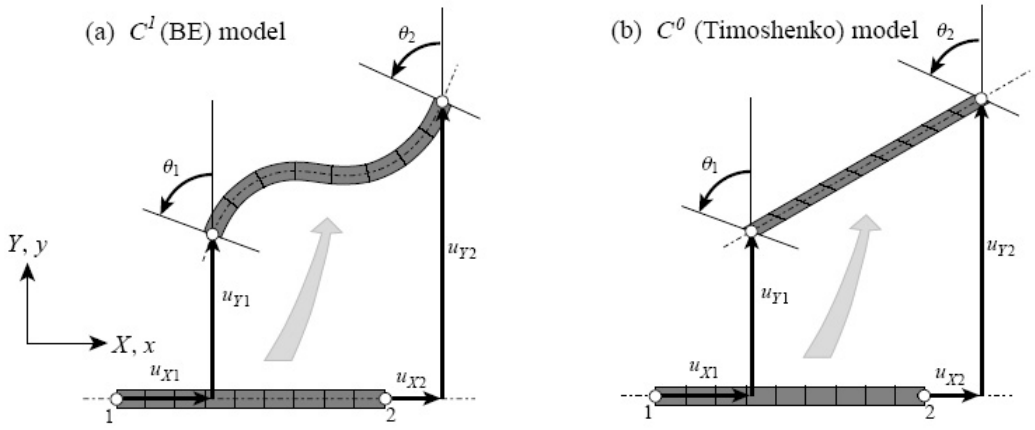

Figure 11: The Bernoulli –Euler element vs. the Timoshenko element (source: [10])

The Timoshenko beam element from [8] is depicted in Figure 12 in undeformed configuration (with length l_0) and in deformed configuration (for clarity, the deformed configuration is depicted as a curved line). The local reference frame in the deformed configuration is defined so that the local x-axis coincides with the neutral axis of the deformed element. And since deflection is described by a linear shape function, the only non-zero deformations in the local reference frame are the elongation of the element (u) and the rotation of the cross-section (ϕ). The deflection of the element is taken into account in the orientation of the local reference frame with respect to the global reference frame, denoted by the angle θ.

The element nodal deformation vector in global coordinates is denoted $\underline{D}_e = (U_i, V_i, \Phi_i, U_j, V_j, \Phi_j)^T$ and due to the choice of local reference frame the element nodal deformation vector in local coordinates is reduced to $\underline{d}_e = (\phi_i, u_j, \phi_j)^T$. By inspection of Figure 12 and Figure 13, the two are related as follows [8]:

$$\underline{d}_e(\underline{D}_e) = \begin{bmatrix} \phi_i \\ u_j \\ \phi_j \end{bmatrix} = \begin{bmatrix} \Phi_i - \theta \\ \sqrt{(U_j - U_i + l_0 \cos\Phi_0)^2 + (V_j - V_i + l_0 \sin\Phi_0)^2} - l_0 \\ \Phi_j - \theta \end{bmatrix} \tag{8}$$

and the finite rotation angle θ is defined in terms of U and V as:

$$\theta = \sin^{-1} \frac{V_j - V_i + l_0 \sin\Phi_0}{\sqrt{(U_j - U_i + l_0 \cos\Phi_0)^2 + (V_j - V_i + l_0 \sin\Phi_0)^2}} \tag{9}$$

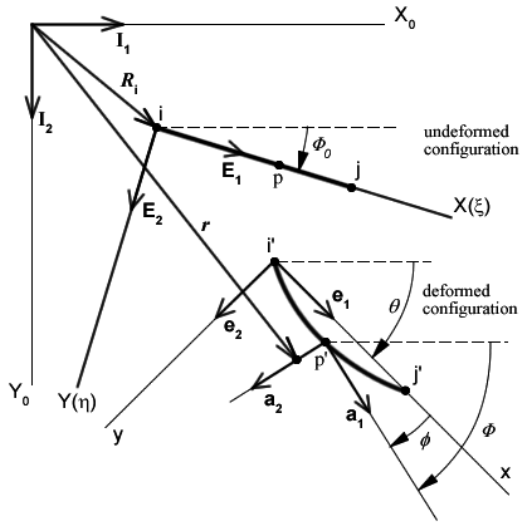

Figure 12: Definition of reference frames (source:[8])

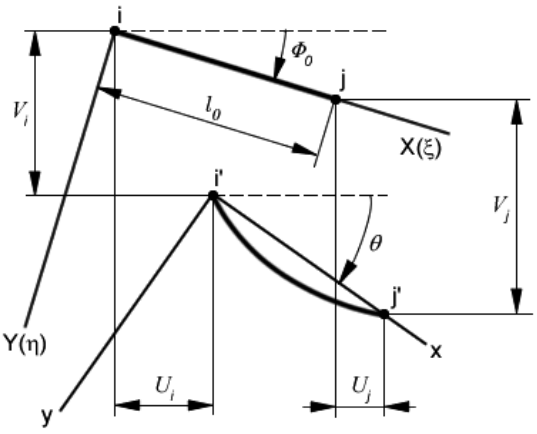

Figure 13: Global displacement relations

2.2 Equations of motion

The equations of motion for the beam element can be determined with the help of Hamilton's principle. Therefore the kinetic energy and potential energy expressions T and V need to be established. The kinetic energy is best determined in terms of global coordinates, whereas the internal potential energy is best determined using local coordinates because the deformation of the beam element is defined with respect to the local reference frame. Referring again to [8] for derivations, the expressions for the kinetic energy T and the internal potential energy $\mathrm{V}_{\mathrm{int}}$ are:

$$\mathrm{T} = \tfrac{1}{2}\underline{D}_e^T \mathbf{M}_e \underline{D}_e \tag{10}$$

$$\mathrm{V}_{\mathrm{int}} = \tfrac{1}{2}\underline{d}_e^T \mathbf{k}_0 \underline{d}_e = \tfrac{1}{2}\underline{d}_e(\underline{D}_e)^T \mathbf{k}_0 \underline{d}_e(\underline{D}_e) \tag{11}$$

In these expressions, $\mathbf{M}_e$ is the global element mass matrix and $\mathbf{k}_0$ is the local element stiffness matrix.

According to [8], the standard consistent mass matrix for the Timoshenko element corresponding to global coordinates is:

$$\mathbf{M}_e = \frac{m}{6}\begin{bmatrix} 2A & 0 & 0 & A & 0 & 0 \\ 0 & 2A & 0 & 0 & A & 0 \\ 0 & 0 & 2I_z & 0 & 0 & I_z \\ A & 0 & 0 & 2A & 0 & 0 \\ 0 & A & 0 & 0 & 2A & 0 \\ 0 & 0 & I_z & 0 & 0 & 2I_z \end{bmatrix} \tag{12}$$

here m is the mass per unit length, A is the cross-sectional area and I_z is the area moment of inertia of the cross-section.

The local stiffness matrix for the Timoshenko element according to [8] is:

$$\mathbf{k}_e = \begin{bmatrix} \frac{4+12\beta_{RBF}}{1+12\beta_{RBF}}\frac{EI_z}{l_0} & 0 & \frac{2-12\beta_{RBF}}{1+12\beta_{RBF}}\frac{EI_z}{l_0} \\ 0 & \frac{EA}{l_0} & 0 \\ \frac{2-12\beta_{RBF}}{1+12\beta_{RBF}}\frac{EI_z}{l_0} & 0 & \frac{4+12\beta_{RBF}}{1+12\beta_{RBF}}\frac{EI_z}{l_0} \end{bmatrix} \tag{13}$$

where $\beta_{RBF} = \frac{EI_z}{GA_s l^2}$ represents the residual bending flexibility method which is employed to prevent shear locking. Here A_s is the shear reduced cross-sectional area, E is Young's modulus and G is the shear modulus of the material.
Application of Hamilton's principle yields the following equations of motion [8]:

$$\mathbf{M}_e \underline{\ddot{D}}_e + \underline{K}_e(\underline{D}_e) = \underline{F}_e \tag{14}$$

where $\underline{K}_e(\underline{D}_e)$ is the nonlinear internal force vector which results from the internal potential energy expression and $\underline{F}_e$ represents the external loads. The internal force vector is best evaluated using symbolic computation software.
The element matrices and vectors can be combined using standard finite element assembly techniques to form the equations of motion for the complete system. These equations of motion can be integrated using a standard time integration scheme. In this paper a fourth order Runge-Kutta scheme is used.

2.3 External loads

In order to simulate a rotor blade under forced flapping conditions, the Timoshenko element described above is used to represent a hinged-free beam. This beam is subjected to three types of loads: a centrifugal load, an aerodynamic load and a forced flapping load.
The centrifugal load and aerodynamic load are represented by nodal forces based on the models depicted in Figure 14 and in Figure 15 respectively. The centrifugal load vector is derived using energy equivalence, while the aerodynamic load is evaluated at the element mid-point and then distributed evenly over the nodes.

Based on the following centrifugal load distribution along the global X coordinate:

$$p_c = \rho A \Omega^2 X \tag{15}$$

the equivalent centrifugal load vector for the beam element becomes:

$$\underline{F}_{e,centr} = \rho A \Omega^2 l_0 \cos\theta \left(\frac{X_i}{2} + \frac{1}{6} l_0 \cos\theta, \quad 0, \quad 0, \quad \frac{X_i}{2} + \frac{1}{3} l_0 \cos\theta, \quad 0, \quad 0 \right)^T \tag{16}$$

where X_i is the global X coordinate of the first node of the element.

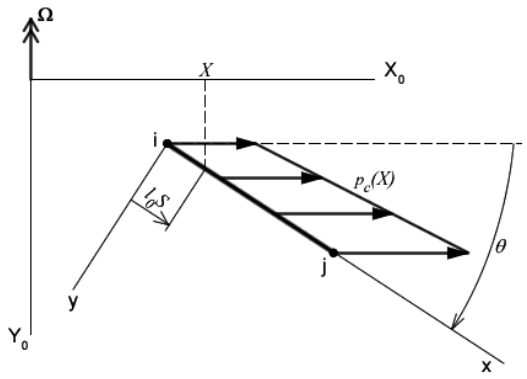

Figure 14: Centrifugal load model

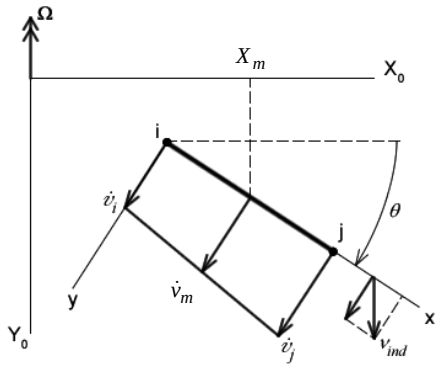

Figure 15: Aerodynamic load model, with velocity distribution normal to the element

The aerodynamic force vector is found using Figure 15 and Figure 6, based on simple blade element theory. The centre of the element is located at:

$$X_m = \frac{X_i + X_j}{2} \tag{17}$$

The airspeed encountered by the element at this point is defined by:

$$V_m^2 = (\Omega X_m)^2 + (v_{ind}\cos\theta - \dot{v}_m)^2 \tag{18}$$

and by inspection of Figure 6 the angle of attack can be expressed as:

$$\alpha_m = \theta_0 - \varphi = \theta_0 - \tan^{-1}\frac{v_{ind}\cos\theta - \dot{v}_m}{\Omega X_m} \tag{19}$$

where φ is the local inflow angle, v_{ind} is the induced airspeed at the element, $\dot{v}_m$ is the local normal component of the absolute velocity of the element centre, and θ_0 is the collective pitch. Assuming a symmetric airfoil with chord c and constant lift slope $\overline{C}_{l_\alpha}$, the lift over an element of length l_0 evaluated at the mid point can then be expressed as:

$$L_m = \overline{C}_{l_\alpha}\alpha_m q_m c l_0 = \overline{C}_{l_\alpha}\left(\theta_0 - \tan^{-1}\frac{v_{ind}\cos\theta - \dot{v}_m}{\Omega X_m}\right)\frac{1}{2}\rho_{air}V_m^2 c l_0 \tag{20}$$

If an asymmetric airfoil is used, the airfoil lift coefficient can be approximated using:

$$\overline{C}_l = \overline{C}_{l_\alpha}(\alpha_m - \alpha_{L=0}) \tag{21}$$

where $\alpha_{L=0}$ is the zero-lift angle of attack.

Assuming a constant average profile drag coefficient $\overline{C}_{d_p}$ the profile drag evaluated at the mid point becomes:

$$D_m = \overline{C}_{d_p}\frac{1}{2}\rho_{air}V_m^2 c l_0 \tag{22}$$

With the help of the local inflow angle φ, the resultant aerodynamic force can be expressed in terms of a component N_m normal to the element and a component T_m parallel to the shaft plane:

$$N_m = L_m\cos\varphi - D_m\sin\varphi \tag{23}$$

$$T_m = L_m\sin\varphi + D_m\cos\varphi \tag{24}$$

The lumped aerodynamic force vector expressed in global coordinates then becomes:

$$\underline{F}_{e,aero} = \left(0, \quad \frac{N_m}{2}, \quad 0, \quad 0, \quad \frac{N_m}{2}, \quad 0 \right)^T \tag{25}$$

and the element contribution to the shaft torque is:

$$Q_{e,sh} = X_m T_m \tag{26}$$

The forced flapping load can be applied at any node by defining a nodal force vector $\underline{F}_{flap}$ as a function of time. Alternatively, a flapping mechanism can be incorporated in the FE discretization, prescribing the motion displacement of a single node as a function of time. The total external force vector is then equal to the sum of the centrifugal force vector, the aerodynamic force vector and the flapping load vector.

2.4 Verification and validation of the FE model

The implementation of the geometrically nonlinear Timoshenko beam element in Matlab has been verified by reproducing some of the test cases presented by [8]. The implementations of the centrifugal force model and the aerodynamic force model have been verified by comparing the FE results for a free flapping rotor blade with the results found using analytical rigid blade theory. Furthermore, the flapping behaviour found using the FE model has been compared with both the rigid blade theory and the flexible blade theory described earlier. On all accounts the qualitative results were satisfactory. For details refer to [7].
Of course it is all very nice to have a model of an Ornicopter rotor blade that does what it should do in a qualitative sense. However, the question remains whether the quantitative results found using the FE model are anywhere near what happens in reality. Therefore the FE model has been used to simulate the rotor blade behaviour of the Ornicopter demonstrator model, and results are compared here with experimental data available.
To this end, a detailed representation of the structural properties and aerodynamic properties of the rotor blade used on the Ornicopter demonstrator is required. This rotor blade, a “Vario” model helicopter blade for use on a four bladed rotor, is a glass fibre composite blade with an asymmetrical airfoil and no twist. Since no detailed information is available for this blade, the values of important parameters had to be determined experimentally. The rotor blade, together with the pitch bearings and attachment to the flapping hinge, is represented by a planar beam with properties varying along the length as depicted in Figure 16.

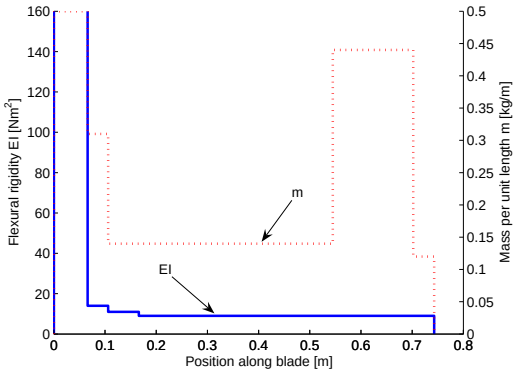

Figure 16: Distribution of mass and flexural rigidity along the Ornicopter demonstrator model blade (including root attachment)

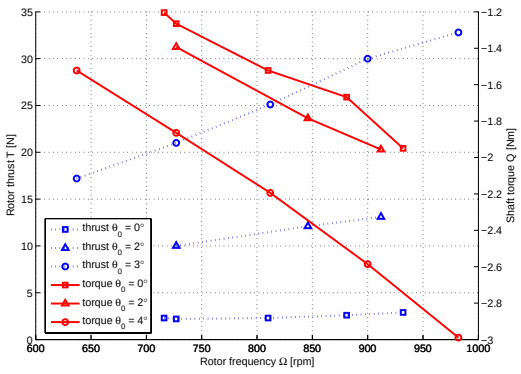

Figure 17: Experimental data available from the Ornicopter demonstrator model in free flapping configuration [6]

In order to obtain a good initial approximation of the distribution of mass m and flexural rigidity EI along the blade length, a blade was cut into small pieces which were then measured and weighed. The flexural rigidity distribution was then fine tuned by fitting the deformed blade shape under static loading conditions to the deformation measured in static loading experiments [9].
The average aerodynamic coefficients for the blade airfoil are based on experimental data obtained from fixed base tests with the radio controlled Ornicopter demonstrator model in free flapping configuration. These data, described by [6], are depicted in Figure 17. It should be noted that the coefficients determined from these data show quite a large variation due to for example the effects of low Reynolds number. In the FE model however, constant values are assumed for the lift slope $\overline{C}_{l_\alpha}$, the lift coefficient at zero angle of attack $\overline{C}_{l_0}$, and for the profile drag coefficient $\overline{C}_{d_p}$. This introduces some errors, but the results have shown to be quite reasonable.

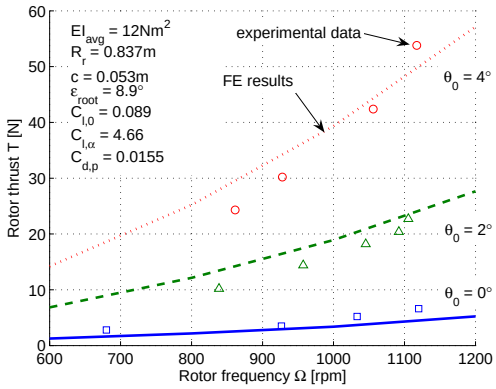

Figure 18: Validation of thrust using experimental data from the Ornicopter demonstrator model. EI_{avg} is the average flexural rigidity of the rotor blade, R_r is the rotor diameter, c is the blade chord and ε_{root} is the root flapping angle

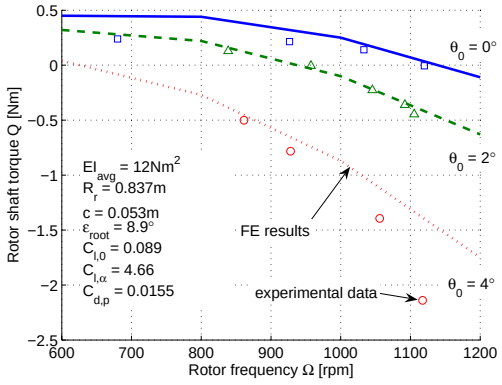

Figure 19: Validation of reaction torque (shaft torque) using the experimental data from the Ornicopter demonstrator model

The FE simulation results for the forced flapping case with an $8.9°$ root flapping angle at different rotor frequencies are depicted in Figure 18 and Figure 19. These figures also show the experimental data obtained from [6]. As expected, some errors occur. The thrust is overestimated at low rpm and underestimated at high rpm (higher Reynolds number). The torque is overestimated for the zero pitch case at low rpm and it is underestimated for the $4°$ pitch case at high rpm. These errors can be attributed mostly to the fact that constant aerodynamic coefficients are used. Furthermore, the tip loss factor can be of influence and possibly the proximity of the experimental model to the ground could also affect the results. Another possible source of errors is that the measurement of the collective pitch angles during the experiments was not very accurate, due to play in the pitch control system. The measurement error in pitch angle can be as large as $\pm 0.5°$.
Nevertheless, the figures show quite a good prediction of rotor thrust as well as shaft torque. Especially the important points where the shaft torque is reduced to zero are predicted quite well.

Thus, if experimental data for a conventional rotor are available and if these are used to fine tune the parameters of the FE model, the FE model can predict the flapping amplitudes required for torqueless rotation with reasonable accuracy. The validation was performed using experimental data obtained from a small model rotor operating at relatively low Reynolds numbers ($2 \cdot 10^5 < \mathrm{Re} < 4 \cdot 10^5$). For a full scale rotor the effects of low Reynolds numbers will be less pronounced, so that the accuracy of the predictions is expected to improve. Furthermore, the calculations will usually be performed for a fixed rotor speed, making the estimation of aerodynamic parameters easier.
This implies that the FE model can be employed to study the behaviour of a rotor blade in the hover condition and that the results can be trusted not only in a qualitative sense, but also in a quantitative sense, if model parameter values are based on accurate experimental data.

3 EVALUATION OF FLAP FORCING METHODS

3.1 Description of flap forcing methods

Now that the FE model has been validated, it can be used to study the effects of different flap forcing methods on the flapping behaviour of a rotor blade. To illustrate this, two flap forcing methods have been analyzed and compared. These flap forcing methods are depicted in Figure 20.
The first method is root flap forcing, as implemented in the Ornicopter demonstrator model. A flapping moment M_{fl} is applied at the location of the flapping hinge. This method will probably lead to very large stresses due to bending moments in the root.
The other method is axial flap forcing. A flapping force F_{fl} is applied in a direction parallel to the rotor shaft at a certain distance from the flapping hinge. This method is expected to yield a more favourable stress distribution in the blade.

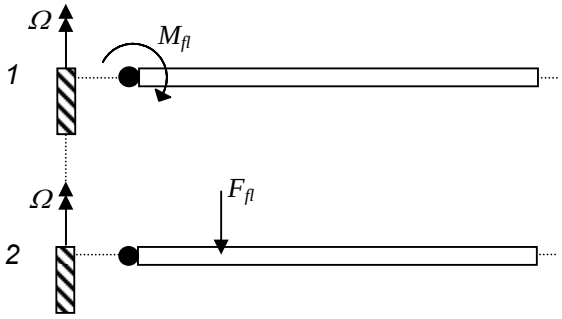

Figure 20: Flap forcing load cases for a blade with hinge offset

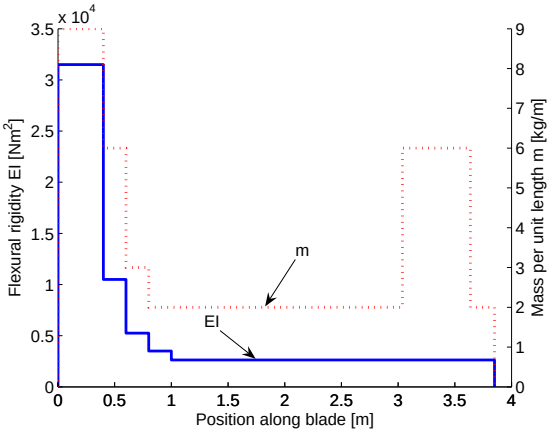

Figure 21: Distribution of mass and flexural rigidity along the blade

These flap forcing load cases have been applied to a full scale rotor blade similar to that of a Schweizer 300C helicopter. The calculations have been performed for the hover condition, using an aircraft mass of 900kg and a rotor speed of 470rpm. The rotor blades are assumed to be made of aluminium 2014, prismatic from the root outwards, without twist and using a symmetrical NACA 0015 airfoil. The blade has a length of 3.85m. The actual distribution of flexural rigidity and mass along the blade length is not known. Therefore a distribution

similar to that of the model rotor blade is used. The average flexural rigidity of a Schweizer 300C rotor blade, according to experiments, is equal to 3500Nm^2 [7]. Based on this value and assuming that the root of the blade is reinforced, the distribution of Figure 21 results. A hinge offset of 0.4m was used in the calculations and the force in Case 2 was applied at 0.4m from the hinge.
For each flap forcing case, the displacement amplitude of the load application point and the load amplitude required for torqueless rotation have been determined. The corresponding stress distributions in the blade have also been determined in order to gain insight into Ornicopter rotor blade design requirements.

3.2 Flapping amplitudes and flapping loads required for torqueless rotation

The blade is subjected to a sinusoidal load with amplitude $\hat{M}_{fl}$ in Case 1 or $\hat{F}_{fl}$ in Case 2 (Figure 20) and frequency Ω (1-P excitation). The deformed shapes of the blade at the moment of maximum tip deflection and at the moment of maximum root amplitude are depicted in Figure 22 for Case 1 and in Figure 23 for Case 2. The corresponding rigid blade result is also shown, as a reference. Note that the deformations are exaggerated in these figures due to the scale of the vertical axis.

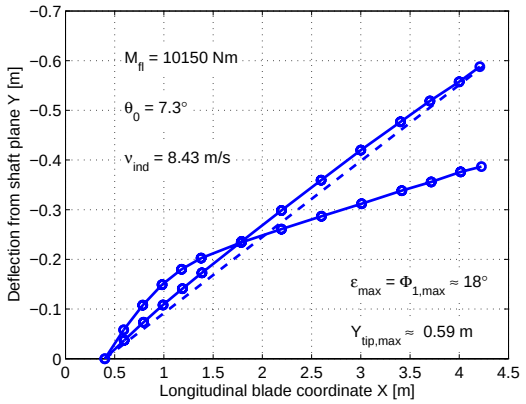

Figure 22: Deformed blade for Case 1, with a moment applied to the first node. The two instances represent maximum root deflection and maximum tip deflection. The dashed line represents rigid blade theory for a centrally hinged blade.

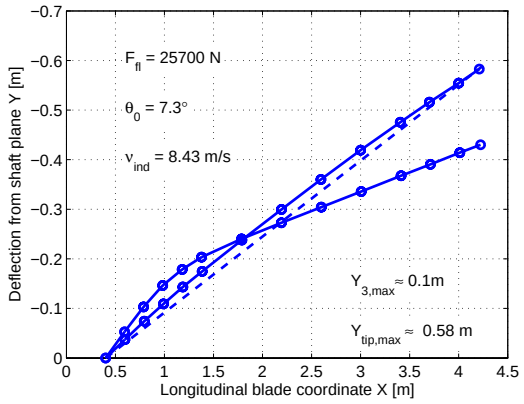

Figure 23: Deformed blade for Case 2, with a force applied in vertical direction to the third node. The two instances represent maximum root deflection and maximum tip deflection.

The maximum tip displacement of the blade in both cases approaches the value found using rigid blade theory. The root flapping angle in both cases becomes larger than the rigid blade angle, as expected. The ratio of flexible blade root amplitude and rigid blade amplitude is approximately $\hat{\varepsilon}_{flex} / \hat{\beta}_{rigid} \approx 2.2$ for both cases, whereas the analytical two-mode approximation predicts a ratio of 3.2 (for a uniform centrally hinged blade without lift). The flapping moment of 10150Nm found in Case 1 is smaller than the rigid blade value of 14198Nm, as expected.
At first sight, there does not appear to be much difference between the two cases in terms of blade deformation, although the blade does bend a bit more in Case 1. However, the difference between the two flap forcing methods becomes clear when looking at the stress distributions.

3.3 Stress distribution in the blade

The normal stress distribution along the length of the blade, in the lower skin and in the upper skin, is depicted in Figure 24 for Case 1 and in Figure 25 for Case 2. This is the stress at the moment in time at which maximum bending deformation occurs. The figures also show the stress distribution for the same blade in free flapping, as a reference. Note that for a free flapping blade, the stress in the upper skin is almost the same as in the lower skin, hence only one line is shown. The corresponding deformed blades are shown in Figure 26. Note that, unlike Figures 22 and 23, this is scaled correctly.

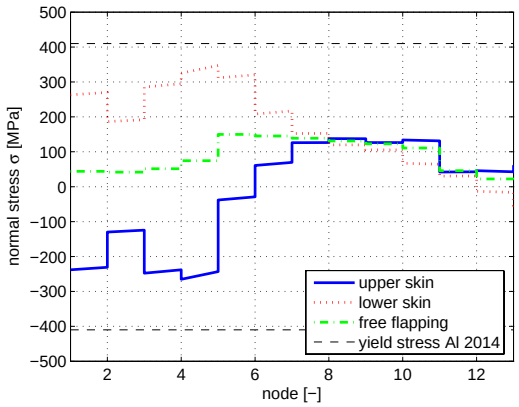

Figure 24: Normal stress along the blade length in the upper and lower skin for Case 1. The stress in the blade during free flapping is also shown.

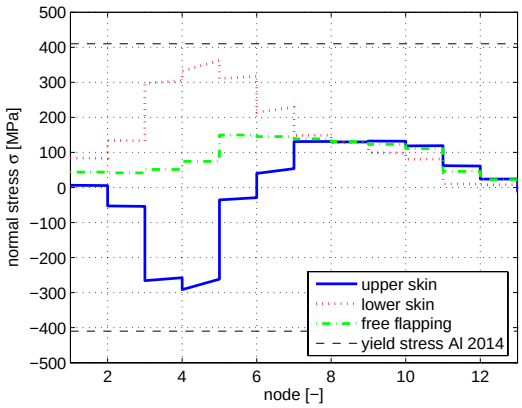

Figure 25: Normal stress along the blade length in the upper and lower skin for Case 2. The stress in the blade during free flapping is also shown.

When looking at the outboard part of the blade (nodes 7-13), it appears that the stress distributions in both cases are almost equal to the distribution in the free flapping blade. The inboard part of the blade on the other hand does show large stress levels in both forced flapping cases.
The influence of load application method becomes clear here. Although the maximum normal stress in Case 2 (flapping force) becomes slightly larger than in Case 1 (flapping moment), the stress level near the root is much smaller. This is consistent with expectations.

Nevertheless the maximum stress levels are twice as high as in the free flapping case. These stress levels come dangerously close to the yield stress for aluminium 2014 which is depicted as a reference. Taking into account the fact that this is an oscillating load, it becomes apparent that fatigue will probably be a major issue in the design of Ornicopter rotor blades.
To illustrate this, assume a fatigue limit of 25% of the ultimate stress. For aluminium 2014 this would be 120MPa. The maximum normal stress in the blade is approximately 360MPa (Figure 25). According to a typical endurance curve for aluminium, the blade would not even last for 10^4 cycles. At a rotor speed of 470rpm (8Hz) the blade would fail after 21minutes. Thus, the (fictional) blade, as it is presented here, will not be able to cope with the oscillating stresses predicted.
Even though the structural properties of the blade used in these calculations do not accurately represent a real blade, it becomes clear that a rotor blade for the Ornicopter will need to be specially designed to cope with the flapping loads. With fatigue in mind, probably composite blades would be a better choice than aluminium blades.

All in all, this shows that the FE method presented here can be used as a qualitative tool for the preliminary design of Ornicopter rotor blades and flapping mechanisms. If reliable data about the structural properties and aerodynamic properties are available, the quantitative results will also show reasonable accuracy.

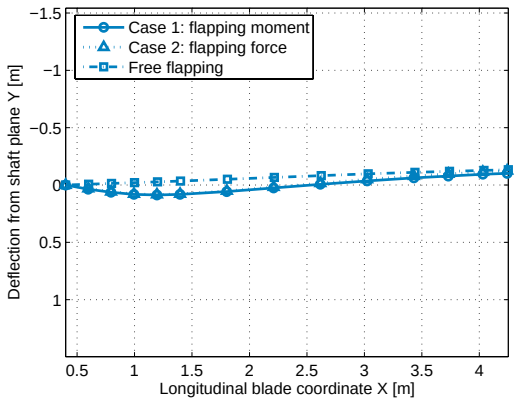

Figure 26: Deformed blades corresponding to the stress diagrams, at the moment that maximum stress occurs. Note that the axes now have the same scale.

4 CONCLUSIONS

This paper stresses the importance of accurate prediction of forced flapping amplitudes and forced flapping loads for the design of Ornicopter flapping mechanisms and rotor blades. It was shown that existing analytical rigid blade theory and analytical flexible blade theory are not very well suited for this purpose.
Therefore an alternative method was presented. This method is based on an implementation of the planar, geometrically nonlinear finite beam element for dynamic analysis presented by [8]. External load models were presented that simulate the centrifugal forces and aerodynamic forces acting on an Ornicopter rotor blade.
It was shown that the finite element method presented is able to predict rotor performance to a reasonable degree, using measurement data obtained from an experimental Ornicopter demonstrator model. With the help of more detailed data for the aerodynamic parameters even better results could probably be obtained.
The finite element method was then employed to evaluate two different flap forcing methods for a full scale rotor using an aluminium rotor blade similar to that of a Schweizer 300C helicopter. The load cases under consideration were: Case 1, flapping moment applied at the flapping hinge and Case2, a flapping force applied parallel to the rotor shaft at approximately 10% from the flapping hinge.
Analysis of the bending deformations showed a root flapping amplitude of approximately two times the value found using rigid blade theory, whereas the analytical flexible blade method predicted a factor three. This result is almost the same for both load cases.
Analysis of the normal stress distribution in the blade shows that, even though Case 2 yields a lower stress level in the root of the blade, both cases experience almost the same maximum stress. This maximum stress is approximately twice as large as the maximum stress that occurs in a free flapping blade. This in itself is not very bad. However, the level of stress together with the fact that it is oscillating at 8Hz is cause for concern with respect to fatigue. It

is concluded that the (fictional) rotor blade presented would fail within 10^4 load cycles. Note however that no attempt has been made to optimize the blade for this type of loading.
In conclusion, the finite element method presented as an alternative to analytical theories yields satisfactory results as long as accurate structural and aerodynamic data are available for the rotor blade under consideration. The method can be used as a tool in the preliminary design of flapping mechanisms and rotor blades for the Ornicopter.

5 REFERENCES

[1] Th. van Holten, "A Single Rotor without Reaction Torque: a Violation of Newton's Laws or Feasible?", 28th European Rotorcraft Forum, Bristol, United Kingdom, 2002

[2] Th. van Holten, M. M. Heiligers, G.J. van de Waal, "The Ornicopter: A Single Rotor without Reaction Torque. Basic Principles.", 24th International Congress of the Aeronautical Sciences, Yokohama, Japan, 2004

[3] Th. van Holten, M. M. Heiligers, "Configuration analysis of a torqueless helicopter concept.", 24th ICAS Congress, Yokohama, Japan, August-September 2004.

[4] Th. van Holten, M. M. Heiligers, "The influence of flexible blades on the characteristics of the Ornicopter.", 30th European Rotorcraft Forum, 2004

[5] Th. van Holten, M. M. Heiligers, R. Kuiper, S. Vardy, G. J. van de Waal, J. Krijnen, "Forced Flapping Mechanisms for the Ornicopter: A Single Rotor Helicopter without Reaction Torque.", 30th European Rotorcraft Forum, Marseille, France, 2004.

[6] S. van den Bulcke, "Design, Manufacturing and Testing of a radio-controlled model Ornicopter.", Master's thesis, Delft University of Technology, Faculty of Aerospace Engineering, Delft, The Netherlands, 2005.

[7] D. J. van Gerwen, "Ornicopter rotor blade behaviour: An investigation into forced flapping.", Master's thesis, Delft University of Technology, Faculty of Aerospace Engineering, Delft, The Netherlands, 2005.

[8] M. Iura, S. N. Atluri, "Dynamic analysis of planar flexible beams with finite rotations by using inertial and rotating frames.", Computers & Structures, Vol. 55 (3), 1995, pp. 453-462.

[9] P. Perdijk, "Blade tests for the Ornicopter model.", Internship report, Delft University of Technology, Faculty of Aerospace Engineering, Delft, The Netherlands, 2005.

[10] C. A. Felippa, "Nonlinear Finite Element Methods.", University of Colorado, Boulder, Colorado, 2001.